

Research paper

Difunctional covalent organic framework hybrid material for synergistic adsorption and selective removal of fluoroquinolone antibiotics



Wei Jiang ^{a,c}, Wei-Rong Cui ^a, Ru-Ping Liang ^{a,1}, Jian-Ding Qiu ^{a,b,* 2}

^a College of Chemistry, Nanchang University, Nanchang 330031, China

^b College of Materials and Chemical Engineering, Pingxiang University, Pingxiang 337055, China

^c Nanchang Institute for Food and Drug Control, Nanchang 330038, China

ARTICLE INFO

Editor: Dr. L. Haizhou

Keywords:

Difunctional covalent organic framework
Hybrid material
Synergistic adsorption
Selective removal
Fluoroquinolone antibiotics

ABSTRACT

Due to the low efficiency of traditional sewage treatment methods, the effective removal of zwitterionic fluoroquinolone (FQs) antibiotics is of vital significant for environment protection. In this work, a SO₃H-anchored covalent organic framework (TpPa-SO₃H) was deliberately designed by linking phenolic trialdehyde with triamine through Schiff reaction, then low-content Tb³⁺ ions were loaded onto covalent organic framework according to wet-chemistry immersion dispersion method which benefitting for efficient FQs antibiotics uptaking. Tb@TpPa-SO₃H functionalized with regularly distributed sulfonic acid groups and terbium ions which could provide difunctional binding sites. Tb³⁺ sites could capture carboxylic acid group of FQs molecules according to the complexes coordination effect and sulfonic acid sites play a significant role in the adsorption of FQs molecules through electrostatic interaction with amine group. Tb@TpPa-SO₃H with dual complementary function sites exhibited ultra-fast adsorption kinetics (< 2 min, average over 99% removing rate) and high adsorption capacities of 989, 956, and 998 mg g⁻¹ for Norfloxacin (NOR), ciprofloxacin (CIP), enrofloxacin (ENR), respectively. Furthermore, Tb@TpPa-SO₃H showed excellent selectivity for the adsorption of FQs in tanglesome system. This work not only explored synergistic adsorption in ion-functionalized 2D covalent organic framework with dual binding sites, but also delineated a promising strategy for the elimination of organic pollutants in environmental remediation.

1. Introduction

Fluoroquinolones (FQs) are probably among the most important synthetic antibiotics agents in veterinary treatment and human medicine worldwide because of their excellent antibacterial activity (Ezellab et al., 2018; Abrusan and Marsh, 2019). However, because of relative ineffectiveness of traditional sewage disposal technology and illegal discharges, FQs have been detected out in various water environment (Van Doorslaer et al., 2014; Luo et al., 2011). Potential hazards arising from improper FQs releasing have gained increasing attention, since direct antibiotics exposure could potentially result in drug resistance and toxic effects to environments (Hess et al., 2019; Abouelhassan et al., 2019; Wang et al., 2014). Removal of FQs from various water environments through relatively green methods with high efficiency is one of the most promising strategies to meet the growing demands for

water treatments. Therefore, novel designment of adsorbents with excellent extraction performance and prominent selectivity based on structure/property relationships of target molecule has attracted tremendous interests for the removal of FQs antibiotics (Zhang et al., 2016; Van de Voorde et al., 2014).

The common molecular structures of FQs antibiotics endow two ion-binding sites which including carboxyl and amine groups. Based on the intrinsic low charge density of amine groups, it inclines to integrate with negative charged soft-base fragment as binding sites in adsorbents, such as sulfonic acid groups (Da et al., 2019; Ahmed et al., 2015; Konwar et al., 2019). Sulfonated absorbent materials, such as sulfonated graphene nanosheets, have been used as the adsorbents for nitrogen-containing compounds removal in wastewater treatment (Shen and Chen, 2015). Unfortunately, these materials exhibit uncontrollable distribution and less few functional sites loading, which severely

* Corresponding author at: College of Chemistry, Nanchang University, Nanchang 330031, China.

E-mail address: jdqiu@ncu.edu.cn (J.-D. Qiu).

¹ Ru-Ping Liang: 0000-0002-2244-3000

² Jian-Ding Qiu: 0000-0002-6793-9499

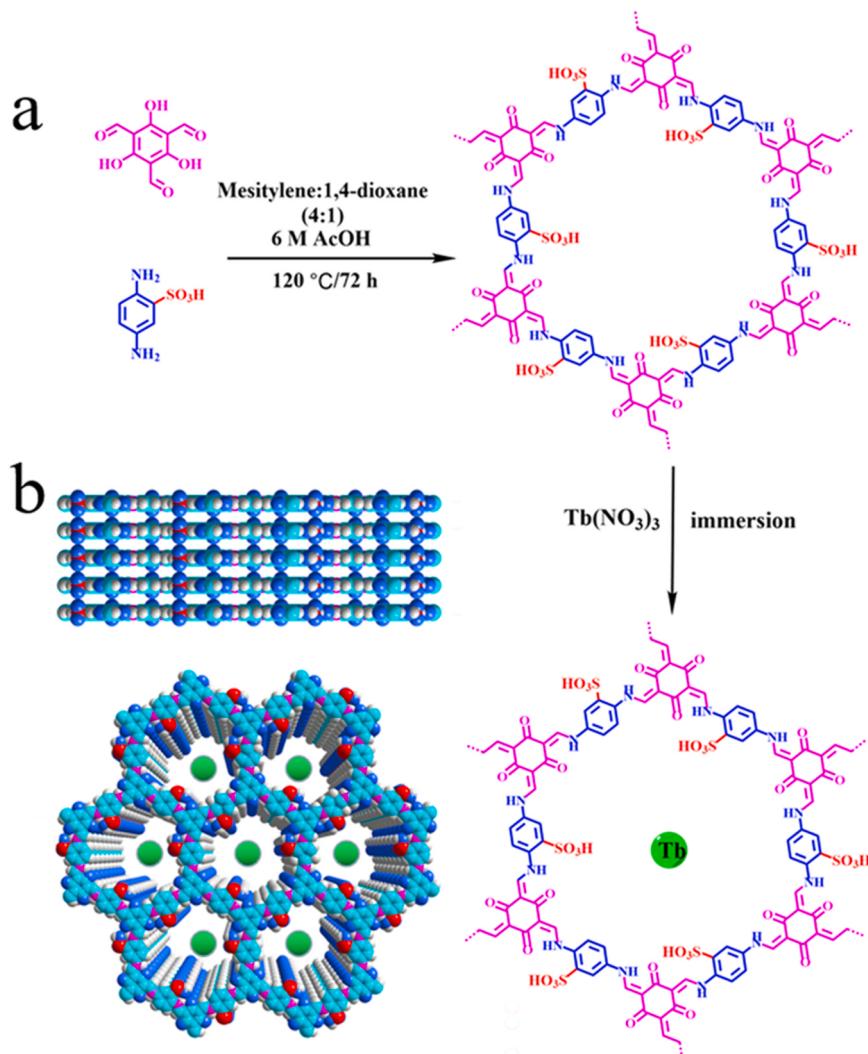


Fig. 1. (a) Scheme diagram for the preparation of Tb@TpPa-SO₃H; (b) Graphic view of the slipped AA stacking structure of Tb@TpPa-SO₃H (magenta, N; blue, O; red, S; cyan, C; white, H; green, Tb) (For interpretation of the references to colour in this figure legend, the reader is referred to the web version of this article).

compromising combining capacity (Shen and Chen, 2015). Ionic metal organic frameworks (iMOFs), have been intensively studied attributing to definite charged functional group and devisable crystalline porous structure (Van de Voorde et al., 2014), for example MIL-101(Cr)-SO₃H shows the highest adsorption capacity to FQs antibiotics among various ionic MOFs (Guo et al., 2019). But relatively low density of functional groups is unfavorable for ionic site accessibility, thus resulting in a low adsorption affinity (Van de Voorde et al., 2014). Meanwhile, these ionic materials are designed to bind amine groups solely, and the binding to amine groups of sulfonic acid was inhibited by the presence of carboxyl, thus further compromising binding capacity (McConnell and Beer, 2012; Hua et al., 2019; Chi et al., 2017). The binding inhibition effect of ionic adsorbents could be diminished by deliberately modification of adsorbents endowed with a functional group to bind with the carboxyl simultaneously (McConnell and Beer, 2012; Wang et al., 2019).

It was reported that composite materials which loaded with metal on the surface were one of the highest effective adsorbents for oxygen acid (Setyono and Valiyaveetil, 2014; Muthu Prabhu et al., 2018). Loading metals as electro-deficient functional groups could improve the affinity for highly electronegative species through complexation or ligand substitution (Setyono and Valiyaveetil, 2014). Terbium (Tb) oxides nanoparticles as fluorometric reagents have been developed for the determination of salicylate, lasalocid, and tetracycline (Castillo-Garcia et al., 2012). Besides terbium-based coordination polymer nanoparticles

were used as adsorbents for the extraction and detection of ciprofloxacin in tablets and biological fluids (Tan et al., 2013). Considering the typical chemical structures of FQs antibiotics with a highly electronegative carboxyl group, assembling electro-deficient functional groups by metal loading could further improve the affinity and selectivity of adsorbents for FQs antibiotics. Hence, the incorporation of terbium ion in crystalline porous materials is expected to harness the porous structure and construct a double functional group for synergistic enhancement in the affinity and selectivity of adsorption.

Ionic covalent organic frameworks (iCOFs) with charged organic units are new subclass of COFs with prominent electrostatic functionality (Geng et al., 2020; Huang et al., 2017; Cui et al., 2020). The flexibly adjustable structures of iCOFs empower precise integration of tremendous predesignable ionic sites into framework (Cui et al., 2020). In two-dimensional (2D) iCOFs, the charged layered structures stack through π - π interactions and form one-dimensional (1D) pore channel aligning along the stacking orientation (Geng et al., 2020; Huang et al., 2017). Thus, the ionic sites can be uniformly distributed, and the number of ionic sites can be accurately regulated. The porous crystalline structure of iCOFs promotes the Tb³⁺ to be evenly dispersed (Ding et al., 2011; Lu et al., 2017). Meanwhile, the weak stability of the Tb³⁺ complex can be made up by iCOFs with good chemical and thermal stabilities (Geng et al., 2020). These traits suggested that Tb³⁺-functionalized iCOFs hybrid material can be precisely devised for high-efficiency and

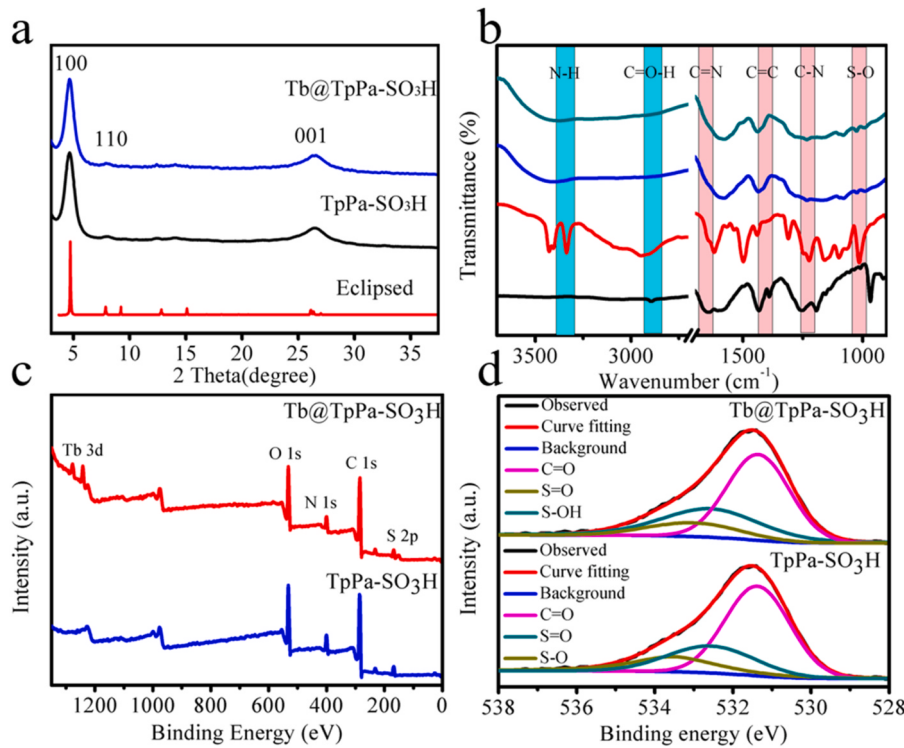


Fig. 2. (a) PXRD patterns of simulated TpPa-SO₃H and Tb@TpPa-SO₃H; (b) FTIR spectra of Tp (black curve), Pa-SO₃H (red curve), TpPa-SO₃H (blue curve) and Tb@TpPa-SO₃H (cyan curve); (c) survey spectrum of TpPa-SO₃H (blue curve) and Tb@TpPa-SO₃H (red curve); (d) O 1 s of TpPa-SO₃H and Tb@TpPa-SO₃H (For interpretation of the references to colour in this figure legend, the reader is referred to the web version of this article).

outstanding selectivity sorbent of FQs antibiotics.

In this study, Tb@TpPa-SO₃H was prepared for efficient and selective trapping of FQs antibiotics. Sulfonic acid groups were homogeneously introduced to the surface of iCOFs and low-content Tb³⁺ was loaded subsequently to generate difunctional binding sites for businesslike removal of FQs antibiotics, thus dual binding mechanism including complementary electrostatic and coordination effect was produced between the Tb@TpPa-SO₃H and FQs antibiotics. The Tb@TpPa-SO₃H showed fast adsorption kinetics with high removal efficiency (99.0%) in 2 min and record-high adsorption capacities of 989, 956, and 998 mg g⁻¹ toward norfloxacin (NOR), ciprofloxacin (CIP), enrofloxacin (ENR), respectively. In addition, Tb@TpPa-SO₃H exhibited high selectivity to separate FQs antibiotics in tanglesome system containing diversiform competitive organic compounds and natural seawater with high salinity. This research offered a prospective strategy for the designs of the ion-functionalized 2D COF hybrid material for organic pollutants adsorption and other environmental remediation fields.

2. Materials and methods

2.1. Chemicals and materials

All reagents and solvents were used without further purification unless otherwise mentioned. 1,3,5-triformylphloroglucinol (Tp, 97%), 2,5-diaminobenzenesulfonic acid (Pa-SO₃H, 97%), terbium(III) nitrate pentahydrate (Tb(NO₃)₃·6 H₂O, 99.9%), norfloxacin (NOR), ciprofloxacin (CIP), enrofloxacin (ENR), sulfamethoxazole (SMZ), cefalexin (CL) and oxolinic acid (OA) were purchased from the Aladdin Bio-Chem Technology Co., Ltd. Tetrahydrofuran (THF), acetic acid (HAc, 99%), and N,N-dimethylformamide (DMF) were obtained from Sinopharm Chemical Reagent Co., Ltd.

2.2. Preparation of adsorbent

2.2.1. Synthesis of TpPa-SO₃H

TpPa-SO₃H was synthesized following a reported method with slight modification (Chandra et al., 2016). Briefly, 3 mL mesitylene/1, 4-dioxane (4:1) mixture solution with 1,3,5-triformylphloroglucinol (Tp) (0.3 mmol, 63 mg), 2,5-diaminobenzenesulfonic acid (Pa-SO₃H) (0.45 mmol, 84.6 mg) and acetic acid (0.3 mL, 6.0 M) in a pyrex tube was flash-frozen at 77 K, then the reaction tube was flame-sealed and heated at 120 °C for 3 days. The red solids were resoundingly obtained, and washed several times with N,N-dimethylformamide and tetrahydrofuran, respectively. At last, the final product was dried in a vacuum at 90 °C for 12 h. Except that p-phenylenediamine was used instead of 2, 5-diaminobenzenesulfonic acid, TpPa was synthesized in the same process.

2.2.2. Synthesis of Tb@TpPa-SO₃H

Freshly prepared TpPa-SO₃H (175 mg) was added into 10 mL Tb (NO₃)₃·6 H₂O solution (0.01 M, 0.02 M, 0.06 M, respectively) and soaked for 48 h at room temperature. The product was collected with centrifugation and completely washed with deionized water to remove physically absorbed Tb³⁺ on the surface. At last, the obtained product was dried in vacuum at 90 °C.

2.3. Adsorption experiments

To carry out Tb@TpPa-SO₃H isotherm adsorption experiment, the initial concentration of NOR, CIP, and ENR solution was changed in the range from 10 mg L⁻¹ to 500 mg L⁻¹. 5.0 mg of as-synthesized Tb@TpPa-SO₃H was added into sample bottle which containing 10 mL antibiotics solution, and the solutions were agitated with a constant shaking speed at 180 rpm for 2 h. The remaining concentration of target antibiotics pollutant in the filtrates was analyzed by high-performance liquid chromatography (HPLC). During the adsorption kinetic

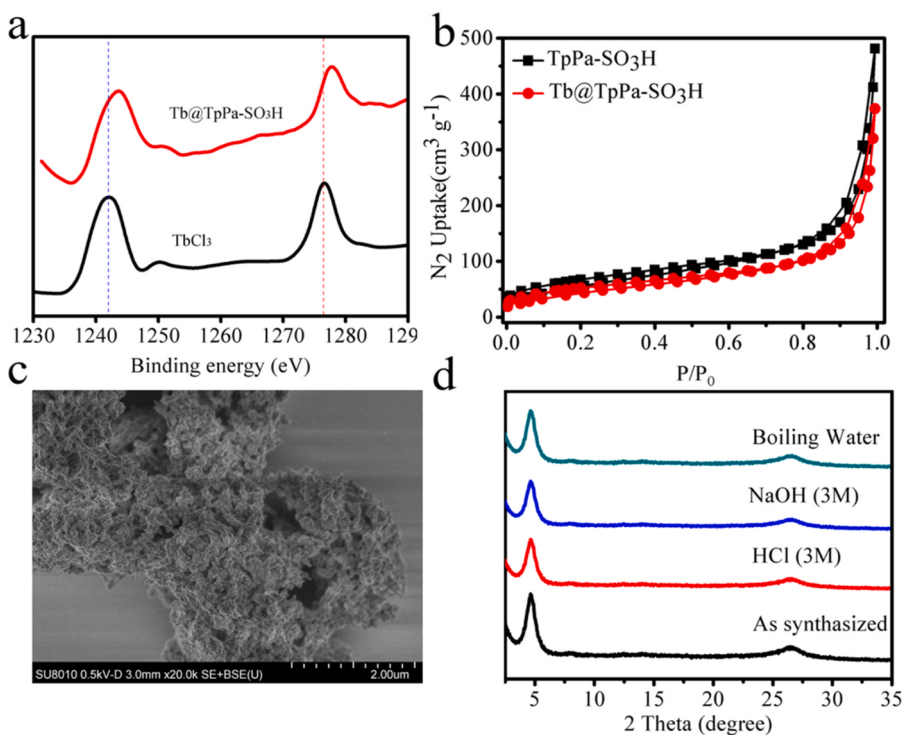


Fig. 3. (a) Binding energy of Tb 3d in TbCl₃ and Tb@TpPa-SO₃H; (b) N₂ adsorption and desorption isotherms of TpPa-SO₃H and Tb@TpPa-SO₃H; (c) SEM image of Tb@TpPa-SO₃H; (d) Stability tests of Tb@TpPa-SO₃H in 3 M NaOH, 3 M HCl, and boiling water.

experiment, 50 mg of as-synthesized Tb@TpPa-SO₃H was added to sample bottle containing 100 mL FQs solution (10 mg L⁻¹) at pH 8.0, and the bottle were put into a shaker at 180 rpm. At different time intervals, the remaining concentrations of antibiotics were quantitatively confirmed after filtration.

3. Results and discussion

3.1. Characterization

Fig. 1a illustrated the scheme for the synthesis of Tb@TpPa-SO₃H by two steps which including the synthesis of TpPa-SO₃H as the matrix materials and Tb³⁺ incorporation by direct immersion. TpPa-SO₃H was synthesized by reacting 2,5-diaminobenzenesulfonic acid (Pa-SO₃H) and 2,4,6-triformylphloroglucinol (Tp) under solvothermal conditions. Sulfuric acid as anionic sites was homogeneously introduced to the surface of COFs for efficiently interaction towards amine groups in antibiotic molecules (Shen and Chen, 2015). The Tb³⁺ as charge-balancing anions inside the pore channels interact with sulfonic acids units slightly, which promoting the uniformly dispersion of Tb³⁺ species (Fig. 1b) (Jansone-Popova et al., 2019). The interfacial interaction between terbium ions and the COF framework is conductive to be exchanged out by NOR due to the intrinsic properties of large size and low charge density of amine groups in FQs molecular (Da et al., 2019). It is important to mention that the adsorption process does not hamper structural integrity of the hybrid material because of the reversible metal sulfonate bond and the ability of the -SO₃ group to offer simultaneous multidirectional ligation (Morris and Brammer, 2017). The terbium ions as electro-deficient functional groups can interaction with carboxyl groups of FQs through complexation, thus further diminishing ion binding inhibition (McConnell and Beer, 2012). Sulfonic acids groups and terbium ions were introduced into the framework to produce difunctional sites. The synergistic difunctional sites in Tb@TpPa-SO₃H contribute to FQs antibiotics trapping with high efficiency and prominent selectivity.

The crystallinity and structure of Tb@TpPa-SO₃H were determined

by the powder X-ray diffraction (PXRD). The distinct PXRD peak at 4.8° can be ascribed to the {100} facet of a regular ordered lattice (Fig. 2a, black curve) (Chandra et al., 2016; Kandambeth et al., 2012). The broad peak at 27.0° assigned to the {001} facet further confirmed the formation of 2D COFs in a crystalline and π-π stacking form (Karak et al., 2018; Huang et al., 2017). The pawley refinement of the AA stacking mode outputting a PXRD profile (Fig. 2a, red curve) fitted well with the experimental result. The AA-stacking mode provides one-dimensional (1D) channel, allowing adjoining alignment of sulfonic acid (Huang et al., 2017; Chandra et al., 2016). This regular spatial arrangement effectively endowed the accessibility of the anionic sites towards FQs (Huang et al., 2017). Tb@TpPa-SO₃H was obtained by Tb³⁺-functionalized TpPa-SO₃H. The PXRD pattern of Tb@TpPa-SO₃H verified that this modification does not hamper the structural integrity and overall crystallinity of the framework (Fig. 2a, blue curve). As shown in Fig. 2b, the diagnostic peaks of aromatic N-H (Pa-SO₃H) at 3437 and 3346 cm⁻¹ (red curve) and 1639 cm⁻¹ of C=O (Tp) (black curve) disappeared, revealing the formation of imine bonds between Pa-SO₃H and Tp (Chandra et al., 2016; Kandambeth et al., 2012). Meanwhile, interestingly the FTIR spectra did not show the typical stretching bands of imine (C=N) groups, which should have been present if the compounds existed in the enol form (Kandambeth et al., 2012). Instead, the keto tautomer is verified by the presence of C=C peak at 1436 cm⁻¹ and the newly absence of C-N bonds in the COF appeared at 1233 cm⁻¹ (Kandambeth et al., 2012). The -SO₃H groups of TpPa-SO₃H was further notarized by the characteristic peak at 1026 cm⁻¹ (Fig. 2b, blue curve) (Chandra et al., 2016). After Tb³⁺ functionalization, the S-O stretching vibration at 1026 cm⁻¹ slight shifted to 1024 cm⁻¹ were ascribed to the effect of interaction between two groups (Fig. 2b, cyan curve). The X-ray photoelectron spectroscopy (XPS) was further used to explore this interaction. Fig. 2c gives the full XPS spectra in the range of 0–1350 eV. Characteristic peak corresponding to Tb³⁺ was observed in the spectra of Tb@TpPa-SO₃H, implying successful loading of Tb³⁺. As depicted in Fig. 2d, the O 1 s core level of S-O (533.5 eV) was shifted to a lower binding energy (533.1 eV) in Tb@TpPa-SO₃H. Meanwhile, the characteristic peaks of Tb 3d revealed a change and shift to higher binding

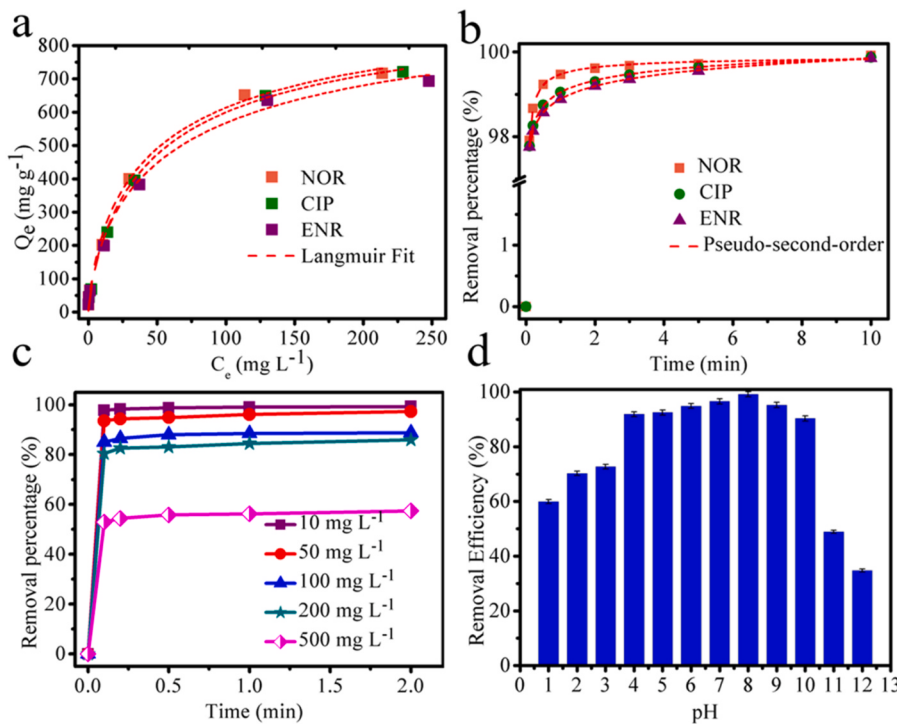


Fig. 4. (a) Adsorption isotherms for FQs on $\text{Tb}@\text{TpPa-SO}_3\text{H}$ (initial concentration was 10, 20, 50, 100, 200, 300, and 500 mg L^{-1} ; and solution volume was 40 mL); (b) Pseudo-second-order kinetics of different FQs on $\text{Tb}@\text{TpPa-SO}_3\text{H}$ (initial concentration was 10 mg L^{-1} ; and solution volume was 100 mL); (c) Adsorption kinetics of $\text{Tb}@\text{TpPa-SO}_3\text{H}$ toward NOR at initial concentrations ranging from 10 mg L^{-1} to 500 mg L^{-1} (solution volume was 100 mL); (d) Removal efficiency of $\text{Tb}@\text{TpPa-SO}_3\text{H}$ toward NOR at different pH conditions (initial concentration was 10 mg L^{-1} and solution volume was 40 mL; ($\text{Tb}@\text{TpPa-SO}_3\text{H}$ was 0.5 g L^{-1} and pH 8.0 for all).

energy after Tb loaded in $\text{TpPa-SO}_3\text{H}$ (Fig. 3a) (Wang et al., 2019). These phenomena could be due to the interaction between sulfonic acid of $\text{TpPa-SO}_3\text{H}$ and terbium ion, which was favorable to the further bifunctional site adsorption process.

The Brunauer-Emmett-Teller (BET) surface areas of $\text{TpPa-SO}_3\text{H}$ was 236 $\text{m}^2 \text{ g}^{-1}$, and $\text{Tb}@\text{TpPa-SO}_3\text{H}$ showed similar N_2 adsorption isotherms with $\text{TpPa-SO}_3\text{H}$, but the BET surface area reduced to 182 $\text{m}^2 \text{ g}^{-1}$, suggesting the existence of Tb^{3+} inside the pore channels (Fig. 3b) (Wang et al., 2019). The SEM images of $\text{Tb}@\text{TpPa-SO}_3\text{H}$ showed uniform porous morphology (Fig. 3c), favoring the dispersion of Tb^{3+} species. Meanwhile, energy dispersive X-ray spectroscopy (EDS) was conducted to further confirm the distribution of Tb^{3+} ions in the $\text{Tb}@\text{TpPa-SO}_3\text{H}$. As shown in Fig. S1, Tb element was uniformly distributed in elemental map. $\text{Tb}@\text{TpPa-SO}_3\text{H}$ was dispersed in multifarious extreme conditions to explore structural stability. After being treatment with boiling water solutions, NaOH (3 M), and HCl (3 M) for 24 h, $\text{Tb}@\text{TpPa-SO}_3\text{H}$ still maintained high crystallinity and excellent chemical stability through PXRD (Fig. 3d) and FTIR spectroscopy (Fig. S2) tests (Kandambeth et al., 2012). The Tb content of filter liquor was monitored by the inductively coupled plasma mass spectrometry (ICP-MS) after treatment with different pH conditions, ethanol, acetonitrile, tetrahydrofuran, and N,N-dimethylformamide (Table S1 and Table S2), no visible Tb peeling-off occurs thus confirming interfacial interactions between Tb^{3+} and $\text{Tb}@\text{TpPa-SO}_3\text{H}$, which is favorable for subsequent recycling and preventing secondary environmental pollution. The TGA curves of $\text{TpPa-SO}_3\text{H}$ and $\text{Tb}@\text{TpPa-SO}_3\text{H}$ demonstrated that they remained thermally stable up to 300 °C (Fig. S3). The defects of the weak stability of the Tb^{3+} complex can be made up by the good chemical and thermal stabilities of iCOFs, which greatly improving the adhesion between $\text{Tb}@\text{TpPa-SO}_3\text{H}$ and FQs antibiotics.

3.2. Adsorption performance

3.2.1. Adsorption isotherms

To investigate optimum dosage of Tb^{3+} loading in $\text{TpPa-SO}_3\text{H}$, the adsorption capacity of hybrid material with different dosage of Tb^{3+} loading for NOR were tested through batch adsorption experiments. The

hybrid materials prepared were labeled based on mole ratio of the Tb ion and $\text{TpPa-SO}_3\text{H}$ [$\text{Tb}^{0.5}@\text{TpPa-SO}_3\text{H}$, $\text{Tb}^1@\text{TpPa-SO}_3\text{H}$, and $\text{Tb}^3@\text{TpPa-SO}_3\text{H}$, corresponding to the mole ratio of Tb ion to $\text{TpPa-SO}_3\text{H}$ at 0.5, 1, and 3, respectively]. As showed in Fig. S4, $\text{Tb}^1@\text{TpPa-SO}_3\text{H}$ possessed highest adsorption capacity compared to $\text{Tb}^{0.5}@\text{TpPa-SO}_3\text{H}$ and $\text{Tb}^3@\text{TpPa-SO}_3\text{H}$. It can be seen that due to the increase of available active sites, the removal capacity increased with the increasing of Tb^{3+} loading dose. The adsorption capacity reached highest value at $\text{Tb}^1@\text{TpPa-SO}_3\text{H}$. When the loading dose continued to increase, the removal capacity was decreased due to the depletion of active sulfonic acid adsorption sites (Fig. S5, Table S3). Therefore, $\text{Tb}^1@\text{TpPa-SO}_3\text{H}$ (hereafter termed as $\text{Tb}@\text{TpPa-SO}_3\text{H}$ for simplicity) was used for all experiments unless otherwise mentioned. With the high correlation coefficient (R^2), it can be seen that the experiment data showed better compliance with the Langmuir model (Fig. 4a and Table S4), implying that the uniform and monolayer adsorption model was more suitable for FQs sorption process (Peng et al., 2018). Generally, a material with a distribution coefficient value (K_d) value more than 10^4 mL g^{-1} is deemed as an excellent remover (Feng et al., 2018). NOR as a typical contaminant of zwitterionic FQs antibiotics was chosen for further study. The K_d of $\text{Tb}@\text{TpPa-SO}_3\text{H}$ towards NOR at 25 °C was $2.38 \times 10^6 \text{ mL g}^{-1}$ (Table S5), indicating the strong affinity between $\text{Tb}@\text{TpPa-SO}_3\text{H}$ and NOR. The saturated adsorption capacity toward NOR was 989 mg g^{-1} , higher than most previously reported porous adsorbents (Table S6). This should be ascribed to $\text{Tb}@\text{TpPa-SO}_3\text{H}$ containing high-density functional sites and erratic pore distribution, which significantly improving the adsorption capacity of NOR (Nassar et al., 2019; Wan et al., 2018). $\text{Tb}@\text{TpPa-SO}_3\text{H}$ gave higher adsorption capacity than ionic MOFs such as cationic MOFs ZIF-8 (Zhou et al., 2019) and anionic MIL-101(Cr)-SO₃H (Guo et al., 2019). The adsorption capacity of ZIF-8 and MIL-101(Cr)-SO₃H for NOR adsorption are 63 mg g^{-1} and 408.2 mg g^{-1} , respectively (Guo et al., 2019; Zhou et al., 2019). Its outstanding adsorb ability was principally due to the synergistic interaction between antibiotics and $\text{Tb}@\text{TpPa-SO}_3\text{H}$ via difunctional sites implanting (Paul et al., 2012). The introduction of terbium ion as functional site for binding the carboxyl simultaneously could diminish ion inhibition, hence improving the accessibility for adsorbents.

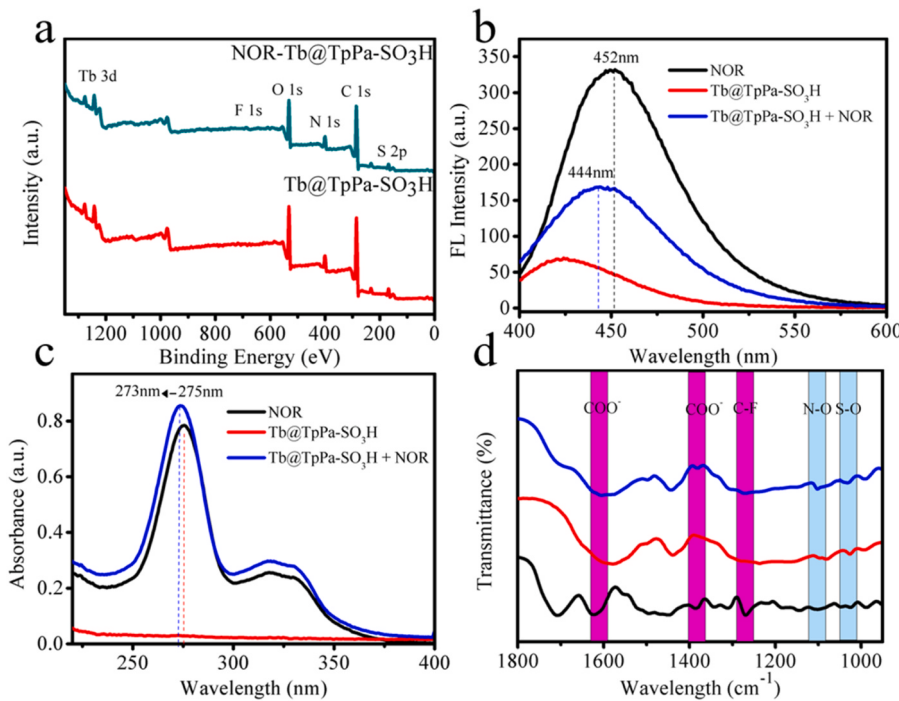


Fig. 5. (a) Survey spectrum of Tb@TpPa-SO₃H and NOR-Tb@TpPa-SO₃H; Fluorescence spectra (b) and UV absorption spectra (c) of free NOR, Tb@TpPa-SO₃H and NOR-Tb@TpPa-SO₃H complex. (d) Comparison of FTIR spectra of Tb@TpPa-SO₃H without (red curve) and with (blue curve) the adsorption with NOR (black curve) (For interpretation of the references to colour in this figure legend, the reader is referred to the web version of this article.).

3.2.2. Adsorption kinetics

The adsorption kinetics were well matched with the pseudo-second-order model (Fig. 4b), revealing that the interactions between the Tb@TpPa-SO₃H and FQs antibiotics were mainly controlled by chemical processes, which might be attributed to the electrostatic interaction (Wang et al., 2019). To access the adsorption kinetics, the Tb@TpPa-SO₃H were mingled with NOR solutions at initial concentrations ranging from 10 to 500 mg L⁻¹ at pH 8. As shown in Fig. 4c, 10 mg L⁻¹ of NOR solution was rapidly decreased by 99.0% in 2 min, revealing the fast adsorption kinetics of Tb@TpPa-SO₃H for FQs. The pseudo-second-order rate constants (k_{obs}) of NOR, CIP, and ENR are 12.96, 8.05, and 6.66 g mg⁻¹ min⁻¹, respectively (Table S7) (Karak et al., 2019). Its outstanding removal rate constant was higher than those of reported porous adsorbents (Table S6), such as commercial activated carbon (1.1×10^{-9} g mg⁻¹ min⁻¹) (Liu et al., 2011), poly-dopamine microspheres (1.53×10^{-3} g mg⁻¹ min⁻¹) (Wan et al., 2018), MIL-101 (Cr) (1.23×10^{-2} g mg⁻¹ min⁻¹) (Bayazit et al., 2017) and MIL-101(Cr)-SO₃H (0.135 g mg⁻¹ min⁻¹) (Guo et al., 2019). It should be attributed to the structural advantage of difunctional sites, inducing much faster cooperative bindings than ion MOF with single charged groups (McConnell and Beer, 2012). Meanwhile, Tb@TpPa-SO₃H containing high-density ionic sites was favorable for exposing more functional sites compared to typical MOF with relatively low-density ionic sites (Mal et al., 2018).

3.2.3. Effect of solution pH

From the perspective view of practical application, capturing antibiotics in a wide pH range is greatly essential. The influence of pH on the adsorbability for NOR was measured in the range of 1–12 (Fig. 4d). The adsorption efficiencies of Tb@TpPa-SO₃H toward NOR were over 90% within a broad pH range from 4 to 10. The adsorption efficiencies reach the maximal value at pH 8.0. The zwitterionic NOR was chiefly formed at this pH (Fig. S6a-b), suggesting that the double binding mechanism was more consistent with the adsorptive features between Tb@TpPa-SO₃H and NOR.

3.3. Regeneration

The housed NOR could be readily dislodged from the NOR-loaded Tb@TpPa-SO₃H samples with an aqueous solution of ultrapure water containing 5% ammonia at room temperature. After five adsorption-desorption cycles, no apparent diminution in the adsorbability of Tb@TpPa-SO₃H for NOR (100 mg L⁻¹) was detected (Fig. S7). The PXRD, FTIR, and SEM results showed that there was no variation in the holistic structure after five adsorption-desorption cycles (Fig. S8, Fig. S9, and Fig. S10). XPS analysis of Tb@TpPa-SO₃H before and after the adsorption of NOR was carried out to further prove the stability during the adsorption process. Fig. 5a gives the full XPS spectra in the range of 0–1350 eV. No extra peaks were observed in the spectra of Tb@TpPa-SO₃H before and after NOR adsorption, indicating no impurities formed. The Tb content of Tb@TpPa-SO₃H and filter liquor after five cycles were quantitatively confirmed by ICP-MS measurement (Table S8), the results proved negligible Tb decreasing, further confirming the structural stability of hybrid material in this work. These excellent performances endowed Tb@TpPa-SO₃H with great advantage of ecological protection and economy in the removal of FQs antibiotics.

3.4. Adsorption mechanism

The adsorption is particularly relying on the porous structures. Namely, the pore structure on the pore wall surface, is vital important for activating interactions between guests and pores, as the pores constitutes the surfaces that communicates with guest molecules (Geng et al., 2020). Fluorescence spectrum were adopted to demonstrate the interaction between Tb@TpPa-SO₃H and NOR. As depicted in Fig. 5b, NOR solution emitted blue fluorescence at 452 nm under excitation at 330 nm. When Tb@TpPa-SO₃H was mingled with the solution of NOR, the fluorescence intensity of NOR at 452 nm was obviously quenched and the characteristic absorption peak was obviously blue-shifted to 444 nm, which could be ascribed to the formation of the NOR-Tb@TpPa-SO₃H complex (Wu and Tong, 2018). The interaction was further confirmed by UV-vis spectra. As shown in Fig. 5c, while Tb@TpPa-SO₃H

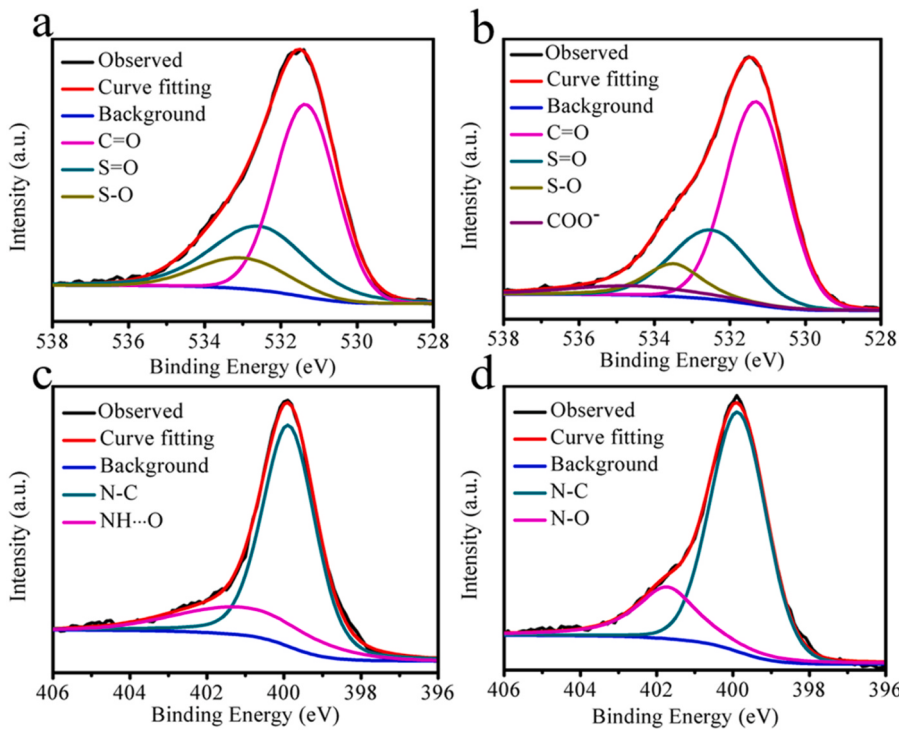


Fig. 6. O 1s XPS spectra of Tb@TpPa-SO₃H (a) and Tb@TpPa-SO₃H-NOR (b); N 1s of Tb@TpPa-SO₃H (c) and Tb@TpPa-SO₃H-NOR (d).

were mingled with the solution of NOR, the characteristic peak of NOR showed slight hypsochromic shift (from 275 to 273 nm). The high-intensity peak located at 275 nm can be assigned to the carboxylate group (Wu and Tong, 2018; Trivedi and Vasudevan, 2007). The changes of absorption peak clearly indicated that Tb³⁺ interacted with the carboxylate group of NOR.

FTIR spectra and XPS were utilized to further explore the interaction between Tb@TpPa-SO₃H and NOR. Comparing FTIR spectra of Tb@TpPa-SO₃H before and after adsorption with NOR, the presence of C-F peak at 1269 cm⁻¹ is in a good agreement with the results of high adsorption capacities of NOR because all the F element coming from NOR molecules (no F element in Tb@TpPa-SO₃H) (Fig. 5d). Meanwhile, compared with individual Tb@TpPa-SO₃H, a new peak at 1624 cm⁻¹ was found from Tb@TpPa-SO₃H coexisting with NOR in FTIR spectra (Fig. 5d). This new peak could be ascribed to COO⁻ stretching vibration of NOR, which is a characteristic peak of NOR-metal ion complex (Tan et al., 2013). In addition, the spectra of O 1 s XPS analysis were consistent with the presence of complexation process as the new peak of COO-Tb (534.8 eV) appeared in Tb@TpPa-SO₃H-NOR (Fig. 6a-b) (Wang et al., 2019; Ning et al., 2019). Besides, the disappearance of COO⁻ stretching vibration peak for COO⁻ at 1380 cm⁻¹ and the appearance of characteristic peak for COO⁻ at 1374 cm⁻¹ were observed in NOR-Tb@TpPa-SO₃H. This indicated that COO⁻ was participated in the NOR adsorption process (Tan et al., 2013; Trivedi and Vasudevan, 2007). And this interaction was further confirmed by XPS of Tb ions. As shown in Fig. S11, the characteristic peaks of both Tb 3d shifted to higher binding energy after NOR adsorption. Thus, the FTIR and XPS spectra reflected that the formation of NOR-Tb@TpPa-SO₃H complex was resulted from the coordination of carboxylic acid group of NOR with Tb³⁺ ions on the surface of Tb@TpPa-SO₃H.

The typical FTIR spectra of Tb@TpPa-SO₃H before and after NOR adsorption are revealed in Fig. 5d. The appearance of the diagnostic peak for SO-N at 1098 cm⁻¹ and the S-O stretching vibration at 1024 cm⁻¹ shifted to 1029 cm⁻¹ were ascribed to the electrostatic interaction between sulfonic acid of Tb@TpPa-SO₃H and amine from NOR (Chandra et al., 2016). Meanwhile, the XPS analysis was consistent with the results obtained from the FTIR spectra. The diagnostic peaks of

NH...O disappeared, which indicated that the NOR adsorption could occur at sulfonic acid group in Tb@TpPa-SO₃H (Fig. 6c-d). In addition, the new characteristic peak of SO-N (401.7 eV) appeared in Tb@TpPa-SO₃H-NOR (Fig. 6c-d) (Ding et al., 2018) and the O 1s core level of S-O (533.1 eV) shifted to a higher binding energy (533.6 eV) (Fig. 6a-b), further corroborating the presence of electrostatic attraction process. Furthermore, to further explore the role of electrostatic attraction in NOR removal, the zeta potential of TpPa-SO₃H was tested in pH8. TpPa-SO₃H shows a high negative zeta potential (-23.3 mV), implying that it prefers to adsorb contaminants with cationic site such as NOR. The zeta potential after NOR adsorption was also investigated (Fig. S12), and the value of zeta potential increased. The adsorption was attributed to electrostatic effect between cationic NOR and -SO₃H. Thus, the synergistic effects of electrostatic interactions and metal coordination are precisely demonstrated from above results. The effective interaction should be attributed to the privileged structure of high-density and uniformly distributed bifunctional groups on the COF surface, improving the adsorption selectivity and efficiency toward NOR.

To study the effect of different functional groups on the adsorption of fluoroquinolone antibiotics, the adsorption capacity of TpPa-SO₃H without Tb ions and TpPa without any functional groups were tested through adsorption experiments (Fig. S13). The saturation sorption capacity of Tb@TpPa-SO₃H, TpPa-SO₃H, and TpPa toward NOR were 726 mg g⁻¹, 531 mg g⁻¹ and 9.5 mg g⁻¹, respectively (Fig. S14). Tb@TpPa-SO₃H displayed markedly higher adsorption capacity than those of TpPa-SO₃H and TpPa, indicating the important role of difunctional group for adsorption. Dual interactions could be formed between the Tb@TpPa-SO₃H and FQs, leading to high adsorption capacity. Nonetheless, compared with that of Tb@TpPa-SO₃H, the adsorbability of TpPa-SO₃H was relatively low. The discrepancy of adsorption behaviors between Tb@TpPa-SO₃H and TpPa-SO₃H should arise from the existence of Tb ion. This discrepancy reveals that the impact of difunctional group is more hardier than that of onefold electrostatic interactions, further indicating Tb ion play an important role in adsorption. For NOR, the minimum adsorption capacity on TpPa was observed, indicating that both sulfonic acid groups and Tb ions are

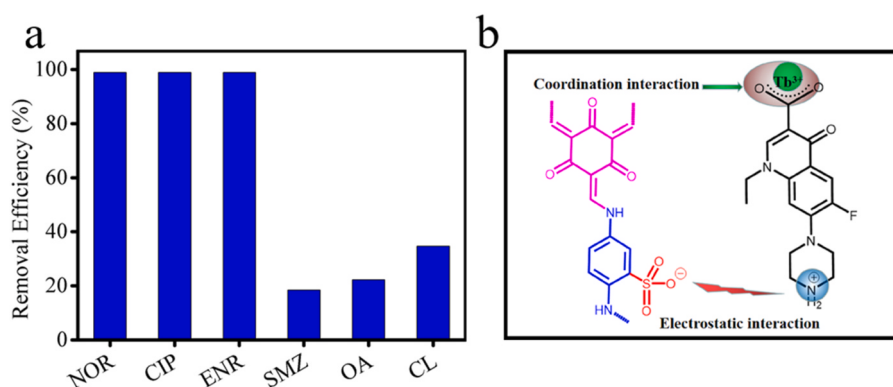


Fig. 7. (a) The adsorption capability of Tb@TpPa-SO₃H towards different contaminants in single component adsorption experiments (initial concentration was 10 mg L⁻¹; Tb@TpPa-SO₃H: 0.5 g L⁻¹; solution volume: 20 mL and pH: 8.0); (b) Proposed mechanism for the removal of FQs by Tb@TpPa-SO₃H.

essential for the effective adsorption of FQ. These results confirmed adsorption of FQs arising from dual effects is featured with muscular binding forces, which may be beneficial to targeted contaminant removal.

To further prove adsorption mechanism, the negatively charged oxolinic acid (OA), sulfamethoxazole (SMZ) with positively charged units, and zwitterionic cefalexin (CL) with zwitterionic units (Fig. S15) were chosen as representative molecules to explore the influence of charges and structure through adsorption experiments. As shown in Fig. 7a, the concentration of NOR, CIP, and ENR decreased from 10 mg L⁻¹ to less than 0.1 mg L⁻¹ within 2 min, which meaning about 99% of pollutants were adsorbed. However, OA, SMZ and CL did not exhibit a noticeable change, only 34.7%, 18.4% and 22.2% were adsorbed respectively due to SMZ and OA solely contained single binding site. It can be seen that the dual interactions only could be formed between the FQs and the Tb@TpPa-SO₃H, thus resulting in outstanding removal efficiency (McConnell and Beer, 2012). However, CL molecules with dual binding sites had relatively lower removal efficiency toward FQs, indicating the spatial orientation and appropriate distance of functional sites played a significant effect (Lin et al., 2018). It showed that adsorption between FQs and Tb@TpPa-SO₃H arising from the dual interaction possessed definite selectivity and powerful binding forces, which may conduce to the environmental application of specific organic molecule extraction.

On the basis of these FTIR, XPS, Fluorescent, and UV-vis results as well as corroborative adsorption experiments, justified adsorption mechanism for the adsorption FQs on the Tb@TpPa-SO₃H was arranged and described in Fig. 7b. The cooperative dual interactions between the terbium ion and sulfonic acids anchored in the Tb@TpPa-SO₃H and the zwitterionic sites of FQs antibiotics strongly enhance the adsorb ability and selectivity of adsorbents. The structures of Tb@TpPa-SO₃H with difunctional sites allowed a high degree of controlment over adsorption processes for FQs.

3.5. FQs extraction from complex system

To assess the potential of Tb@TpPa-SO₃H for practical application, the natural seawater was used as extreme environment to reveal the high selectivity of the designed COF adsorbents for FQs. Removal FQs from seawater is a challenging task due to its relatively low concentration and high concentrations of competing ions which coexisting in the highly complex system. Table S9 showed the prime chemical components of the real seawater, and the concentration of NOR is 61 μ g L⁻¹. In spite of the interfering concentrations of K^+ , Na^+ , Mg^{2+} , Ca^{2+} , SO_4^{2-} , and Cl^- are much greater than targeted NOR, 98.5% of NOR was still removed by Tb@TpPa-SO₃H when the ratio of solid to liquid was 0.5 mg mL⁻¹ (Table S10). At the same time, the concentration of Tb ions in the adsorbent and filtrate after adsorption was measured by ICP-MS

(Table S11). The results showed that the values of metal Tb ion content are basically the same compared with the original adsorbent and seawater, indicating the excellent stability and vast application potential of Tb@TpPa-SO₃H in extreme environments.

4. Conclusion

In this study, we have successfully prepared a difunctional hybrid material Tb@TpPa-SO₃H with record-high adsorption capacities, fast adsorption kinetics and wide pH adaptability towards Fluoroquinolones (FQs) elimination. Tb@TpPa-SO₃H with dual complementary binding sites exhibited excellent performance of molecular separation in the extraordinary complex and high-salinity system which containing abundant competing molecules and ions. FTIR, XPS, fluorescent, and UV-vis spectra analysis elucidated that the adsorption mechanisms were metal coordination and electrostatic interaction simultaneously. Our work promote the investigation of COFs hybrid material with various binding sites to separate organic molecules, further broaden the application of 2D COF hybrid material as adjustable functionalized materials for selective pollutants separation and water environmental remediation.

CRediT authorship contribution statement

Jian-Ding Qiu conceived the research. Jian-Ding Qiu, Wei Jiang, and Ru-Ping Liang designed the research. Wei Jiang performed the synthesis and conducted the experiments. Wei Jiang and Wei-Rong Cui performed the characterizations. Wei Jiang, Jian-Ding Qiu, Wei-Rong Cui, and Ru-Ping Liang participated in drafting the paper and gave approval to the final version of the manuscript.

Declaration of Competing Interest

The authors declare that they have no known competing financial interests or personal relationships that could have appeared to influence the work reported in this paper.

Acknowledgments

This work is supported by the National Natural Science Foundation of China (22036003, 21976077 and 21775065) and the Research Innovation Program for College Graduates of Jiangxi Province (YC2018-B013).

Appendix A. Supporting information

Supplementary data associated with this article can be found in the online version at doi:10.1016/j.jhazmat.2021.125302.

References

- Abouelhassan, Y., Garrison, A.T., Yang, H., Chavez-Riveros, A., Burch, G.M., Huigens 3rd, R.W., 2019. Recent progress in natural-product-inspired programs aimed to address antibiotic resistance and tolerance. *J. Med. Chem.* 62, 7618–7642.
- Abruscan, G., Marsh, J.A., 2019. Ligands and receptors with broad binding capabilities have common structural characteristics: an antibiotic design perspective. *J. Med. Chem.* 62, 9357–9374.
- Ahmed, I., Tong, M., Jun, J.W., Zhong, C., Jhung, S.H., 2015. Adsorption of nitrogen-containing compounds from model fuel over sulfonated metal-organic framework: contribution of hydrogen-bonding and acid-base interactions in adsorption. *J. Phys. Chem. C* 120, 407–415.
- Bayazit, S.S., Danalioglu, S.T., Abdel Salam, M., Kerkez Kuyumcu, O., 2017. Preparation of magnetic MIL-101 (Cr) for efficient removal of ciprofloxacin. *Environ. Sci. Pollut. Res. Int.* 24, 25452–25461.
- Castillo-Garcia, M.L., Aguilar-Caballos, M.P., Gomez-Hens, A., 2012. Application of Tb (4O₇) nanoparticles for lasalocid and salicylate determination in food analysis. *J. Agric. Food Chem.* 60, 11741–11747.
- Chandra, S., Kundu, T., Dey, K., Addicoat, M., Heine, T., Banerjee, R., 2016. Interplaying intrinsic and extrinsic proton conductivities in covalent organic frameworks. *Chem. Mater.* 28, 1489–1494.
- Chi, X., Peters, G.M., Hammel, F., Brockman, C., Sessler, J.L., 2017. Molecular recognition under interfacial conditions: Calix[4]pyrrole-based cross-linkable micelles for ion pair extraction. *J. Am. Chem. Soc.* 139, 9124–9127.
- Cui, W.-R., Zhang, C.-R., Jiang, W., Li, F.-F., Liang, R.-P., Liu, J., Qiu, J.-D., 2020. Regenerable and stable sp³ carbon-conjugated covalent organic frameworks for selective detection and extraction of uranium. *Nat. Commun.* 11, 436.
- Da, H.J., Yang, C.X., Yan, X.P., 2019. Cationic covalent organic nanosheets for rapid and selective capture of perrhenate: an analogue of radioactive pertechnetate from aqueous solution. *Environ. Sci. Technol.* 53, 5212–5220.
- Ding, J., Pu, L., Wang, Y., Wu, B., Yu, A., Zhang, X., Pan, B., Zhang, Q., Gao, G., 2018. Adsorption and reduction of Cr(VI) together with Cr(III) sequestration by polyaniline confined in pores of polystyrene beads. *Environ. Sci. Technol.* 52, 12602–12611.
- Ding, S.Y., Gao, J., Wang, Q., Zhang, Y., Song, W.G., Su, C.Y., Wang, W., 2011. Construction of covalent organic framework for catalysis: Pd/COF-LZU1 in Suzuki-Miyaura coupling reaction. *J. Am. Chem. Soc.* 133, 19816–19822.
- Ezelarab, H.A.A., Abbas, S.H., Hassan, H.A., Abu-Rahma, G.E.A., 2018. Recent updates of fluoroquinolones as antibacterial agents. *Arch. Pharm. Chem. Life Sci.* 351, 1800141.
- Feng, M.L., Sarma, D., Gao, Y.J., Qi, X.H., Li, W.A., Huang, X.Y., Kanatzidis, M.G., 2018. Efficient removal of [UO₂(2+), Cs(+), and Sr(2+) ions by radiation-resistant gallium thioantimonates. *J. Am. Chem. Soc.* 140, 11133–11140.
- Geng, K., He, T., Liu, R., Dalapati, S., Tan, K.T., Li, Z., Tao, S., Gong, Y., Jiang, Q., Jiang, D., 2020. Covalent organic frameworks: design, synthesis, and functions. *Chem. Rev.* 120, 8814–8933.
- Guo, X., Kang, C., Huang, H., Chang, Y., Zhong, C., 2019. Exploration of functional MOFs for efficient removal of fluoroquinolone antibiotics from water. *Microporous Mesoporous Mat.* 286, 84–91.
- Hess, S., Kneis, D., Osterlund, T., Li, B., Kristiansson, E., Berendonk, T.U., 2019. Sewage from airplanes exhibits high abundance and diversity of antibiotic resistance genes. *Environ. Sci. Technol.* 53, 13898–13905.
- Hua, B., Shao, L., Zhang, Z., Liu, J., Huang, F., 2019. Cooperative silver ion-pair recognition by peralkylated pillar[5]arenes. *J. Am. Chem. Soc.* 141, 15008–15012.
- Huang, N., Zhai, L., Xu, H., Jiang, D., 2017. Stable covalent organic frameworks for exceptional mercury removal from aqueous solutions. *J. Am. Chem. Soc.* 139, 2428–2434.
- Huang, N., Wang, P., Addicoat, M.A., Heine, T., Jiang, D., 2017. Ionic covalent organic frameworks: design of a charged interface aligned on 1D channel walls and its unusual electrostatic functions. *Angew. Chem. Int. Ed.* 56, 4982–4986.
- Jansone-Popova, S., Moinel, A., Schott, J.A., Mahurin, S.M., Popovs, I., Veith, G.M., Moyer, B.A., 2019. Guanidinium-based ionic covalent organic framework for rapid and selective removal of toxic Cr(VI) oxoanions from water. *Environ. Sci. Technol.* 53, 878–883.
- Kandambeth, S., Mallick, A., Lukose, B., Mane, M.V., Heine, T., Banerjee, R., 2012. Construction of crystalline 2D covalent organic frameworks with remarkable chemical (acid/base) stability via a combined reversible and irreversible route. *J. Am. Chem. Soc.* 134, 19524–19527.
- Karak, S., Kumar, S., Pachfule, P., Banerjee, R., 2018. Porosity Prediction through hydrogen bonding in covalent organic frameworks. *J. Am. Chem. Soc.* 140, 5138–5145.
- Karak, S., Dey, K., Torris, A., Halder, A., Bera, S., Kanheerampockil, F., Banerjee, R., 2019. Inducing disorder in order: hierarchically porous covalent organic framework nanostructures for rapid removal of persistent organic pollutants. *J. Am. Chem. Soc.* 141, 7572–7581.
- Konwar, L.J., Maki-Arvela, P., Mikkola, J.P., 2019. SO₃H-containing functional carbon materials: synthesis, structure, and acid catalysis. *Chem. Rev.* 119, 11576–11630.
- Lin, S., Zhao, Y., Yun, Y.S., 2018. Highly effective removal of nonsteroidal anti-inflammatory pharmaceuticals from water by Zr(IV)-based metal-organic framework: adsorption performance and mechanisms. *ACS Appl. Mater. Interfaces* 10, 28076–28085.
- Liu, W., Zhang, J., Zhang, C., Ren, L., 2011. Sorption of norfloxacin by lotus stalk-based activated carbon and iron-doped activated alumina: mechanisms, isotherms and kinetics. *Chem. Eng. J.* 171, 431–438.
- Lu, S., Hu, Y., Wan, S., McCaffrey, R., Jin, Y., Gu, H., Zhang, W., 2017. Synthesis of ultrafine and highly dispersed metal nanoparticles confined in a thioether-containing covalent organic framework and their catalytic applications. *J. Am. Chem. Soc.* 139, 17082–17088.
- Luo, Y., Xu, L., Rysz, M., Wang, Y., Zhang, H., Alvarez, P.J., 2011. Occurrence and transport of tetracycline, sulfonamide, quinolone, and macrolide antibiotics in the Haihe River Basin, China. *Environ. Sci. Technol.* 45, 1827–1833.
- Mal, A., Mishra, R.K., Praveen, V.K., Khayum, M.A., Banerjee, R., Ajayaghosh, A., 2018. Supramolecular reassembly of self-exfoliated ionic covalent organic nanosheets for label-free detection of double-stranded DNA. *Angew. Chem. Int. Ed.* 57, 8443–8447.
- McConnell, A.J., Beer, P.D., 2012. Heteroditopic receptors for ion-pair recognition. *Angew. Chem. Int. Ed. Engl.* 51, 5052–5061.
- Morris, R.E., Brammer, L., 2017. Coordination change, lability and hemilability in metal-organic frameworks. *Chem. Soc. Rev.* 46, 5444–5462.
- Muthu Prabhu, S., Chuaicham, C., Sasaki, K., 2018. A mechanistic approach for the synthesis of carboxylate-rich carbonaceous biomass-doped lanthanum-oxalate nanocomplex for arsenate adsorption. *ACS Sustain. Chem. Eng.* 6, 6052–6063.
- Nassar, M.Y., Ahmed, I.S., Raya, M.A., 2019. A facile and tunable approach for synthesis of pure silica nanostructures from rice husk for the removal of ciprofloxacin drug from polluted aqueous solutions. *J. Mol. Liq.* 282, 251–263.
- Ning, E., Yang, L., Tu, B., Pang, Q., Li, X., Xu, H., Qi, Y., Li, Q., 2019. Interface construction in microporous metal-organic frameworks from luminescent terbium-based building blocks. *J. Colloid Interface Sci.* 552, 372–377.
- Paul, T., Machesky, M.L., Strathmann, T.J., 2012. Surface complexation of the zwitterionic fluoroquinolone antibiotic ofloxacin to nano-anatase TiO₂ photocatalyst surfaces. *Environ. Sci. Technol.* 46, 11896–11904.
- Peng, D., Jiang, W., Li, F.-F., Zhang, L., Liang, R.-P., Qiu, J.-D., 2018. One-pot synthesis of boron carbon nitride nanosheets for facile and efficient heavy metal ions removal. *ACS Sustain. Chem. Eng.* 6, 11685–11694.
- Setyono, D., Valiyaveettil, S., 2014. Chemically modified sawdust as renewable adsorbent for arsenic removal from water. *Chem. Eng.* 2, 2722–2729.
- Shen, Y., Chen, B., 2015. Sulfonated graphene nanosheets as a superb adsorbent for various environmental pollutants in water. *Environ. Sci. Technol.* 49, 7364–7372.
- Tan, H., Zhang, L., Ma, C., Song, Y., Xu, F., Chen, S., Wang, L., 2013. Terbium-based coordination polymer nanoparticles for detection of ciprofloxacin in tablets and biological fluids. *ACS Appl. Mater. Interfaces* 5, 11791–11796.
- Trivedi, P., Vasudevan, D., 2007. Spectroscopic investigation of ciprofloxacin speciation at the goethite-water interface. *Environ. Sci. Technol.* 41, 3153–3158.
- Van de Voorde, B., Bueken, B., Denayer, J., De Vos, D., 2014. Adsorptive separation on metal-organic frameworks in the liquid phase. *Chem. Soc. Rev.* 43, 5766–5788.
- Van Doorslaer, X., Dewulf, J., Van Langenhove, H., Demeestere, K., 2014. Fluoroquinolone antibiotics: an emerging class of environmental micropollutants. *Sci. Total. Environ.* 500–501, 250–269.
- Wan, Y., Liu, X., Liu, P., Zhao, L., Zou, W., 2018. Optimization adsorption of norfloxacin onto polydopamine microspheres from aqueous solution: Kinetic, equilibrium and adsorption mechanism studies. *Sci. Total. Environ.* 639, 428–437.
- Wang, F.H., Qiao, M., Su, J.Q., Chen, Z., Zhou, X., Zhu, Y.G., 2014. High throughput profiling of antibiotic resistance genes in urban park soils with reclaimed water irrigation. *Environ. Sci. Technol.* 48, 9079–9085.
- Wang, P., Chen, X., Jiang, Q., Addicoat, M., Huang, N., Dalapati, S., Heine, T., Huo, F., Jiang, D., 2019. High-precision size recognition and separation in synthetic 1D nanochannels. *Angew. Chem. Int. Ed.* 58, 15922–15927.
- Wang, S.Y., Fang, L.F., Matsuyama, H., 2019. Electrostatic adsorption behavior of zwitterionic copolymers on negatively charged surfaces. *Langmuir* 35, 9152–9160.
- Wang, W., Gong, N., Yin, H., Zhang, B., Guo, P., Liu, B., Wang, Y.Y., 2019. Two stable terbium-organic frameworks based on predesigned functionalized ligands: selective sensing of Fe(3+) ions and C₂H₂/CH₄ separation. *Inorg. Chem.* 58, 10295–10303.
- Wu, H., Tong, C., 2018. A specific turn-on fluorescent sensing for ultrasensitive and selective detection of phosphate in environmental samples based on antenna effect-improved FRET by surfactant. *ACS Sens.* 3, 1539–1545.
- Zhang, X., Shen, J., Zhuo, N., Tian, Z., Xu, P., Yang, Z., Yang, W., 2016. Interactions between antibiotics and graphene-based materials in water: a comparative experimental and theoretical investigation. *ACS Appl. Mater. Interfaces* 8, 24273–24280.
- Zhou, L., Li, N., Owens, G., Chen, Z., 2019. Simultaneous removal of mixed contaminants, copper and norfloxacin, from aqueous solution by ZIF-8. *Chem. Eng. J.* 362, 628–637.